JOURNAL OF AIRCRAFT
Vol. 45, No. 5, September–October 2008

Transport Aircraft Three-Dimensional High-Lift-Wing Numerical Transition Prediction

J. Perraud,* J. Cliquet,† R. Houdeville,‡ and D. Arnal§
ONERA, 31055 Toulouse, France
and
F. Moens¶
ONERA, 92190 Meudon, France

DOI: 10.2514/1.32529

Laminar-turbulent transition appears in high-lift configurations through instabilities, attachment-line contamination, or separation. Its prediction may improve the estimation of maximum lift and allows the extrapolation from wind-tunnel measurements to flight conditions. This prediction is being inserted within Reynolds-averaged Navier–Stokes codes to become part of standard design procedures. This requires fast and reliable transition-prediction tools, a very difficult issue in itself. This paper presents recent ONERA progress based on three-dimensional coupling between Navier–Stokes and boundary-layer codes and internal transition prediction within the elsA Reynolds-averaged Navier–Stokes software and their application to a typical transport aircraft high-lift wing used as a common test case in the European projects EUROLIFT 1 and 2. In elsA, emphasis is placed on transition prediction in three-dimensional flows, and issues of contamination and relaminarization are discussed but are left for future tests.

Nomenclature

C_D	=	drag coefficient
C_L	=	lift coefficient
C_p	=	pressure coefficient
Hi	=	incompressible shape factor, $\delta * /\theta$
N_T	=	N factor at transition
Q_e, U_e, W_e	=	total, normal and parallel to leading-edge velocity components at the edge of the boundary layer
T_u	=	external flow turbulence level
u, w	=	normal and parallel to leading-edge velocity components in the boundary layer
X, Z	=	normal and parallel to leading-edge directions
x, y, z	=	local coordinate system
$\delta*$, θ	=	boundary-layer displacement and momentum thicknesses
Λ_2	=	Pohlhausen parameter, $(\theta^2/\nu)(\mathrm{d}U_e/\mathrm{d}s)$
ν	=	kinematic viscosity
φ_{eff}	=	effective sweep angle
φ	=	angle between the wave number and the x direction
ψ	=	angle between the wave number and the external velocity vector

Presented as Paper 264 at the 45th AIAA Aerospace Sciences Meeting and Exhibit, Reno, NV, 8–11 January 2007; received 31 May 2007; accepted for publication 15 February 2008.

*Research Engineer, Models for Aerodynamics and Energetic Department; Jean.Perraud@onera.fr. Member AIAA.

†Ph.D. Student, Models for Aerodynamics and Energetic Department; Julien.Cliquet@onera.fr.

‡Research Engineer, Models for Aerodynamics and Energetic Department; Robert.Houdeville@onera.fr.

§Director of Research, Models for Aerodynamics and Energetic Department; Daniel.Arnal@onera.fr. Member AIAA.

¶Research Engineer, Applied Aerodynamics Department; Frederic.Moens@onera.fr. Member AIAA.

I. Introduction

NUMERICAL simulation of high-lift configurations is a key activity for facing demands for improved performance and reduced emission. It is a challenging domain with regard to the economical, technical, and scientific impacts it may bring. It requires the modeling of complex 3-D multi-element wings, including geometrical details, wing deformation under load, prediction of various types of flow separation, and the modeling of transition, including Tollmien–Schlichting (TS) and crossflow (CF) instability growths, attachment-line contamination, relaminarization, and short bubble separation and transition. As is being demonstrated in the course of the European EUROLIFT 2 project, design based on a purely numerical approach is becoming possible, although wind-tunnel testing remains necessary for final validation and optimization. Because these tests are not usually carried out at flight Reynolds numbers, extrapolation from wind tunnel to flight Reynolds number is needed, requiring a precise understanding of the physical processes involved. One phenomenon playing a major role in this extrapolation is laminar-turbulent transition in its larger acceptance.

The paper presented here is concerned with the validation of transition predictions in full 3-D configurations, internally embedded or externally coupled to the Reynolds-averaged Navier–Stokes (RANS) code elsA. This work is realized by ONERA in the framework of EUROLIFT 2, in a cooperative approach with European research centers and industry. Two aspects under development will be presented: the use of an internal transition-prediction module imbedded in the code and an exploratory 3-D coupling to a 3-D boundary-layer code containing database-type transition-prediction tools.

In the latter case, the difficult point lies in the creation of the proper boundary conditions for the 3-D boundary-layer calculation from the RANS field and without the use of a conical or infinite swept-wing approximation. In such a case, for the RANS mesh to be compatible with the interface, mesh lines should be oriented as normal to the wall and the mesh point density should remain sufficient in the height of the viscous layer. In this process, velocity data are created that allow examining the questions of contamination and relaminarization before computing the boundary layer. As long as the approach is not used iteratively, the transition-prediction tools do not need to be extremely efficient.

In the approach based on a transition-prediction tool inserted into the RANS code, the transition prediction must be as fast as possible because it will become part of the iterative process. Some compatibility conditions must be respected so that transition may evolve in upstream and downstream directions. Computation can be done either along mesh lines or streamlines. In the first case, it is assumed that mesh lines remain globally aligned in the general flow direction, at least in the region of interest. A more general treatment is allowed if following streamlines. Also, it may be necessary to manually determine in which region the flow starts and to indicate domains of influence.

The validation case is a three-element tapered wing called KH3Y, in landing configuration, which was tested in the Airbus-Deutschland low-speed wind tunnel (LSWT) in Bremen, during the EUROLIFT 1 project.

II. Overview of Applied High-Lift Transition Activities in the EUROLIFT Context

Because several parallel developments are being pursued, it is useful to provide some general information on the transition activities. During the EUROLIFT 1 project [1], transition measurements were realized during two experiments. The first one, using the so-called AFV (aile à flèche variable) wing in the ONERA F1 wind tunnel, was dedicated to transition [2]. A detailed experimental database was built on this simplified 3-D high-lift geometry. The evolution of transition location with Reynolds number variation and due to configuration effects (takeoff, landing, and sweep) was measured and analyzed. The second experiment (KH3Y in the LSWT) was a three-dimensional validation experiment with wider objectives [3], preparing other large Reynolds number testing at the European Transonic Wind Tunnel and providing computational fluid dynamics developers with well-documented complex 3-D experimental results.

Concerning transition-prediction tools, several approaches have been investigated in parallel:

1) Based on infinite swept-wing theory, a 2.5-D coupling to RANS surface pressure was initially used to analyze the AFV case [4], which was tested in the ONERA F1 wind tunnel. This provided a validation of contamination and relaminarization criteria and of transition and separation predictions inserted in a boundary-layer code. The ONERA database method for TS and for CF was used in this case.

2) Direct introduction of transition criteria into the elsA RANS code [5] was realized at ONERA and was first applied to the AFV case [6]. This first implementation was then applied to the KH3Y wing, and results are presented here. Work continued after this first demonstration, allowing important extensions [7,8] (multiblock treatment, improved coding, better user control over starting locations, and zones for transition calculation) and resulting in a more robust and simpler treatment of complex cases.

3) The Spanish National Institute for Aerospace Technology (INTA) developed an internal automatic coupling between the structured RANS code EMENS and a boundary-layer code using a conical-wing hypothesis and inserted ONERA database methods for TS and CF instabilities for transition prediction into the boundary-layer code. The methods used and their validation, based on the AFV experiment, are presented in [9].

4) The DLR, German Aerospace Research Center developed an internal automatic coupling between the structured RANS code FLOWer and a boundary-layer code, also using a conical-wing assumption. In 3-D flows, transition prediction is done using a DLR database approach for TS and the ONERA database for CF. The first results were presented in [10]. Validation in the EUROLIFT 2 project has been considered with the KH3Y three-element configuration using the same mesh as in the present paper. Results are available in [11,12].

5) ONERA, the French Aerospace Lab, developed an external interface between the 3-D RANS flow around a tapered wing and the 3-D boundary-layer code 3C3-D to eliminate the need for either the infinite swept or conical-wing assumptions and applied this interface to both the AFV and KH3Y wings. Results for KH3Y are presented here.

In the present paper, only ONERA's results applied to the landing KH3Y case are presented in detail. An overview of results obtained in EUROLIFT 2 with regard to transition prediction and impact, with comparisons of methods and results from the various partners, was presented in [12].

III. Methods for Transition Prediction

In the case of high-lift flows, transition may be caused by several phenomena that need to be modeled. These are attachment-line contamination, short bubble transition, and transition resulting from the growth of instabilities. Relaminarization must also be considered because it may appear downstream of contamination.

A. Attachment-Line Contamination

Attachment-line contamination is due to the transport of floor (or fuselage) turbulence along the attachment line of the wing. Increased sweep angle and large curvature radius in the leading-edge region promote this transport. When this occurs, the whole wing surface becomes turbulent, with no laminar region.

Attachment-line contamination is characterized by the parameter

$$\bar{R} = W_e \Big/ \sqrt{\nu \left(\frac{\partial U_e}{\partial X}\right)_{X_a}}$$

where X_a refers to the attachment line. It can be shown to vary as the square root of the Reynolds number or of the nose radius and increases with sweep angle. The critical value [13,14] of the $\bar{R}$ parameter is usually taken as 250 ± 20.

In the case of an infinite swept-wing assumption, calculation of $\bar{R}$ first requires the knowledge of the effective sweep angle φ_{eff}, from which $W_e = Q_\infty \sin(\varphi_{\text{eff}})$ is obtained. An iterative method may be used for this purpose, looking for a linear evolution with a distance to the attachment line of the normal to leading-edge velocity $U_e = \sqrt{Q_e^2 - W_e^2}$. The location of this attachment line is determined in the process. A similar approach can be used for a conical wing. In the case of direct extraction from the RANS field of the velocity components, $\bar{R}$ can be determined from the velocity gradient at the attachment line, which may usually correspond to a mesh point.

B. Relaminarization

Strong acceleration of a turbulent flow may damp the production terms, to a point that the flow returns to a seemingly laminar state: this is called relaminarization. In 2-D flows, the acceleration parameter

$$K = \frac{\nu}{U_e^2}\frac{\partial U_e}{\partial x}$$

proposed by Beasley [15] is a local parameter, which can be obtained in the preprocessing step, together with attachment-line transition Reynolds number $\bar{R}$. In 3-D flow, K should be evaluated in the streamline direction. Relaminarization of a turbulent boundary layer should be expected if values of K are larger than 5×10^{-6} over a significant distance. Large values have the effect of keeping the boundary layer in a quasi-laminar state, called *laminarescent* [16], but as soon as K decreases, the turbulence reappears rapidly.

Return to turbulence proceeds as in a bypass transition, without going again through a linear stage. Laminar separation of a laminarescent flow may be observed. A turbulent flow is required upstream of relaminarization, which may be caused by contamination.

C. TS and CF Transition from Criteria

In the case of a 3-D base flow, these two criteria are used simultaneously, the first one based on the streamwise component of the velocity and the second one based on the crossflow profile. Transition is considered to occur as soon as one of the two conditions

is realized. These criteria have been used in boundary-layer codes for many years. The longitudinal criterion requires the computation of the incompressible shape factor $Hi = \delta^*/\theta$, a parameter that is often underestimated when computed from RANS viscous velocity profiles [8] (unless special care is taken to ensure an appropriate number of mesh points in the viscous layer). For this reason, an indirect determination, a function of the Pohlhausen parameter, is used in elsA.

The Arnal–Habiballah–Delcourt [17] criterion was developed for the prediction of longitudinal transition caused by TS instabilities. This criterion, based on the same parameters as the Granville criterion, was developed from linear stability analysis of self-similar incompressible velocity profiles ($Hi < 2.7$). The Mack relation $N_T = -8.43 - 2.4\,\ell n(T_u)$ provides the link between the transition location and the external turbulence level. The criterion writes as $R_{\theta_T} - R_{\theta_{cr}} = f(T_u, \bar{\Lambda}_2)$, where

$$\bar{\Lambda}_2 = \frac{1}{x_T - x_{cr}} \int_{x_{cr}}^{x_T} \frac{\theta^2}{\nu} \frac{dU_e}{ds}\, ds$$

is an averaged Pohlhausen parameter; $R_{\theta_{cr}} = \exp(52/H_i - 14.8)$ defines the critical location, the end of the stable region (and the most upstream possible location of transition in a classical approach); and

$$f(T_u, \bar{\Lambda}_2) = -206 \exp(25.7\bar{\Lambda}_2)[\ell n(16.8T_u) - 2.77\bar{\Lambda}_2]$$

This criterion was recently extended to compressible flow.

Transition due to CF instabilities is predicted by means of the C1 criterion [17], based on the crossflow displacement thickness δ_2:

$$R_{\delta_{2_T}} = \frac{300}{\pi} \tan^{-1}\left(\frac{0.106}{(Hi - 2.3)^{2.052}}\right)$$

where

$$\delta_2 = \int_0^{\delta} -\frac{w(y)}{U_e}\, dy$$

D. ONERA Database Methods

Another approach developed at ONERA, referred to as the Arnal–Vialle–Jellitti method [18], provides an estimation of the disturbance growth rate σ of a 2-D compressible boundary layer directly from mean flow parameters and the boundary-layer profile characteristics. The starting idea is that the Reynolds number variation of growth rates obtained solving the exact Orr–Sommerfeld equations can be represented for a given profile and a given frequency using two half-parabolas:

$$\sigma = \sigma_M \left(1 - \left(\frac{R_{\delta_1} - R_M}{R_k - R_M}\right)^2\right) \qquad \begin{array}{ll} R_k = R_0 & \text{if } R_{\delta_1} < R_M \\ R_k = R_1 & \text{if } R_{\delta_1} > R_M \end{array}$$

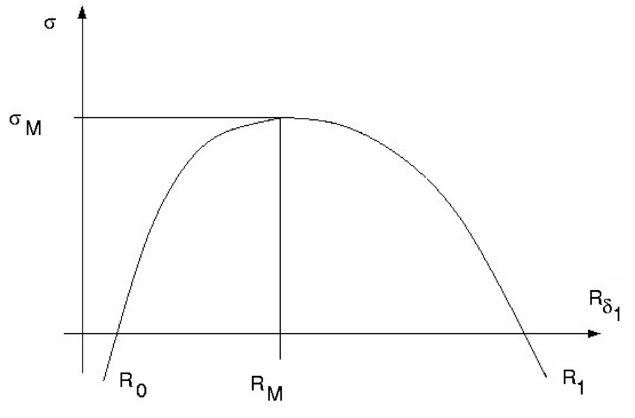

Fig. 1 Growth-rate variations represented using parabolas.

This parabola model (Fig. 1) requires determination of R_0, R_1, R_M, and σ_M as functions of nondimensional frequency $F = (2\pi f\nu/U_e^2)$ (where f is the physical frequency), boundary-layer characteristics, and mean flow conditions. These functions were established from sets of exact stability solutions of Falkner–Skan self-similar profiles in compressible 2-D flows. A first model was thus created for longitudinal instabilities, based on a lookup table using the values of the incompressible shape factor Hi and the local Mach number Me.

Crossflow instabilities are inflectional in nature: they are determined by the location and characteristics of the velocity-profile inflection point. Considering 2-D similar profiles with reverse flow, it was shown that two parameters, $U_i = u(y_i)$ and $P_i = y_i(\partial u/\partial y)_{y_i}$, where y_i is the location of the highest inflection point, allow representing the growth-rate Reynolds number dependence.

A purely analytical model [19] was built for this purpose, first considering attached Falkner–Skan profiles and later extended based on typical compressible profiles close to the leading edge of a transonic wing. To represent crossflow instabilities, use of Stuart's theorem, as noted in [20], and Gaster's [21] relation are necessary. Stuart's theorem states that in temporal theory and for an incompressible flow, the growth rate σ_ϕ in any direction ϕ can be determined from the stability of the 2-D velocity profile projected in the ϕ direction of the original 3-D profile. The projected profile is defined as $U_\phi = \frac{\alpha}{k}u + \frac{\beta}{k}w$ and $k = \sqrt{\alpha^2 + \beta^2}$, with the reduced frequency $F = 2\pi f\nu/U_\phi^2$. Gaster's relation expresses the spatial growth rate in some φ direction in term of temporal amplification ω_i, group velocity modulus V_g, and direction φ_g:

$$-\sigma_\varphi = \frac{\omega_i}{V_g \cos(\varphi - \varphi_g)}$$

where $\varphi = \psi + \theta$. The final model applies only to progressive crossflow instabilities ($F > 0$) and in a range $|\psi| < \psi_{max} < 90$ deg.

The two models for longitudinal and for crossflow instabilities were later combined. The resulting database method for transition prediction allows, with high efficiency, an estimation of the stability characteristics of 3-D boundary layers. Growth rates obtained are integrated to produce envelope N factors exactly as in the case of exact stability theory. Careful optimization has ensured that, in general, the most amplified frequencies are represented with an error below 10%.

One important advantage of the method is that it does not require any initial values and is thus well adapted for automatic use inside boundary-layer codes. Coupling to a RANS code, on the other hand, is quite difficult because the incompressible shape factor must be evaluated with a good precision in the entire unstable region, and the crossflow criterion needs information about the upper part of the velocity profile, where the mesh density is usually rapidly reducing.

E. Separation

For 2-D short bubble transition, the Gleyzes–Habiballah criterion is applied [22]; it uses an analytical representation of the amplification curves for 2-D Falkner–Skan similar profiles with reverse flow ($H_i > 2.7$). For these profiles, stability results are almost independent of frequency, but mostly depend on the incompressible shape factor. Hence, N factor evolution can be written as

$$N(s) - N(s_1) = \int_{R_{\theta_1}}^{R_\theta} \frac{-2.4}{G(H_i)}\, dR_\theta$$

where $N(s_1)$ is the total growth rate at location $s1$, where $\theta = \theta_t$ and $G(H_i)$ is an analytical expression of only H_i. Transition occurs when $N(s) = NT$, given by Mack's relation.

IV. Short Description of the KH3Y Landing Case

The KH3Y model is a half-plane model equipped with a modern type of wing designed by Airbus-Deutschland in the course of a German National Research project. It was selected for use in the EUROLIFT 1 and 2 projects for tests in a number of configurations, from clean wing to advanced flap system with pylon and nacelle, in

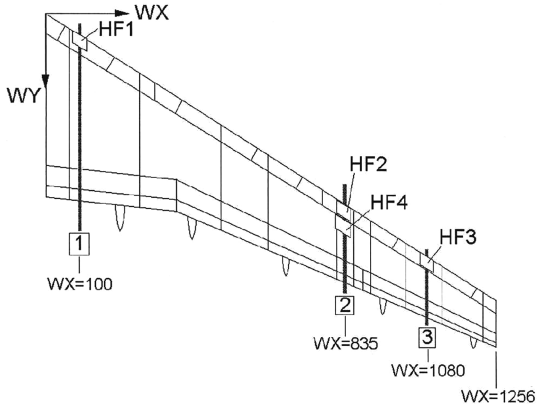

Fig. 2 Planform and hot-film array-locations on the model.

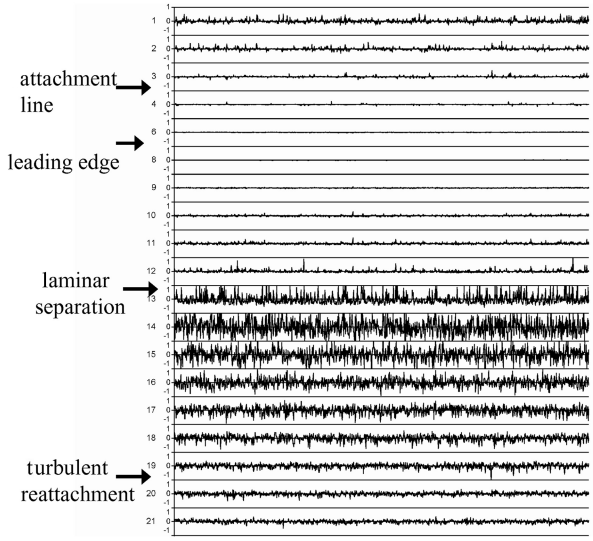

Fig. 3 Typical hot-film signals obtained on HF4 (wing) at a 12-deg angle of attack.

both the Airbus-Deutschland LSWT facility and in the pressurized cryogenic European Transonic Wind Tunnel. The first series of tests at the LSWT [1,3] were realized with a three-element full-span slat and flap wing without nacelle, in both takeoff and landing configurations, at a single chord Reynolds number R_C of 1.35×10^6 and at Mach 0.175. The landing configuration, with slat and flap settings of 26 and 32 deg, respectively, was later selected for transition work because a larger set of transition observations was available in that configuration.

The model was equipped with several arrays of hot films (HF), placed on the carbon fiber slat and on the main wing leading-edge region (Fig. 2), and was observed using two infrared cameras. Analysis focused on the slat and wing hot films located at midspan of the outer wing. Experiments covered the range from 5- to 25-deg angle of attack. Stall was observed around 20 deg from hot-film and infrared-camera observations, and the following evolution was observed:

On the slat, transition is observed (and it is located over the hot-film array) above a 10-deg angle of attack for the upper slat. Laminar separation is observed above 12 deg, leading to rapid transition. Contamination does not seem to be an issue for this element.

On the wing upper side, separation is observed with an angle of attack greater than 4 deg Contamination starts between 10 and 12 deg and, as visible in Fig. 3 at 12 deg, is followed by relaminarization and laminar separation. Figure 3 shows hot-film signals recorded around the wing leading-edge region from the lower side (top trace) to the upper-wing surface (lower trace). Small fluctuations are visible in the attachment-line region and are seen to grow when moving toward the lower side. They are suppressed around the leading-edge region due to relaminarization and then a brutal rise is visible and corresponds to laminar separation. The separation region extends down to a turbulent reattachment. Turbulent traces never reach the level observed within the separation region. On the upper side of this wing, for this Reynolds number, transition is never detected independently of laminar separation. The wing lower side is equipped with just a few hot films, but it is monitored by an infrared camera. Several configurations show quite extensive laminar regions on the lower side at angles of attack below 10 deg, indicating a probable transition through growth of instabilities. There is no available information about transition over the flap.

Based on the experimental results and on a first analysis using experimental pressure measurements, a number of configurations were defined as representative of various phenomena to be modeled. Because natural transition from boundary-layer instability growth was never observed during these tests, it was decided to create one extra case with a chord Reynolds number 3 times larger ($R_C = 4.05 \times 10^6$) and to focus on the two configurations at 10 and 12 deg, as indicated in Table 1. Transition locations indicated in this table reflect the final conclusions of the analysis of experimental results, observations, and computations based on measured pressure distributions.

Thanks to Airbus-Deutschland, a 97-block, 5.5-million-point structured mesh, for which the surface components are shown in Fig. 4, was then created for this wing and provided to the EUROLIFT 2 partners. This mesh was designed to ensure a y^+ smaller than 1. A first series of computations was realized under fully turbulent flow conditions using the Spalart–Allmaras turbulence model in the elsA code. As shown in Figs. 5 and 6, evolutions with angle of attack of the lift coefficient and pressure distribution were close to the experimental results, validating the use of this mesh. Turbulent computation produces a $C_{L\max}$ at 23 deg, instead of 20 deg in the experiment.

V. Three-Dimensional RANS with Internal Transition Prediction

As already explained, motivation for introducing the transition prediction in the RANS calculation is quite strong. Exploratory work demonstrated that precise computation of boundary-layer velocity profiles in RANS requires a far-too-large number of points, especially in 3-D computations. The two remaining possibilities consist of either estimating the boundary-layer integral parameters from the RANS field and using transition criteria or using an automatic coupling to a boundary-layer code that gives access to the boundary-layer profiles at a number of selected wing sections, allowing the use of full or simplified stability analysis for the determination of N factors. The first solution is being developed at ONERA with the elsA code.

Transition-prediction capability has been introduced into the elsA code based on transition criteria that were developed at ONERA for use in boundary-layer codes. A number of criteria have been inserted

Table 1 Case definition for the numerical studies; numerical values refer to X/C locations

	Upper slat X/C	Upper wing	Lower wing
8.5 deg, $Re = 4.05 \times 10^6$	Transition 0.31	Separation	Transition
10 deg, $Re = 1.35 \times 10^6$	Laminar separation 0.11, transition 0.21	Laminar separation 0.08	TS transition
12 deg, $Re = 1.35 \times 10^6$	Laminar separation 0.10, transition 0.14	Contamination, relaminarization, and separation 0.07	Turbulent
14 deg, $Re = 1.35 \times 10^6$	Laminar separation 0.09, transition 0.11	Contamination, relaminarization, and separation 0.05	Turbulent

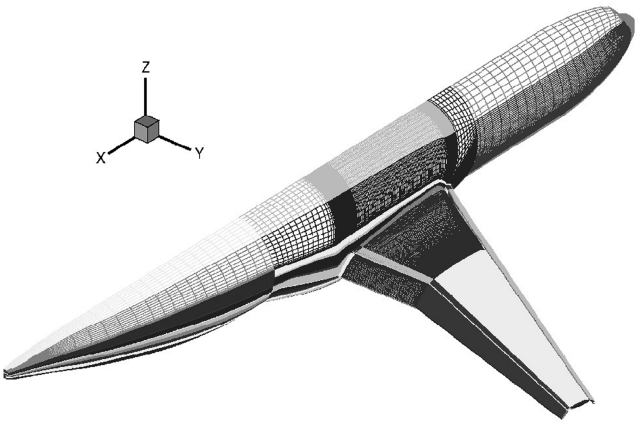

Fig. 4 View of the surface mesh.

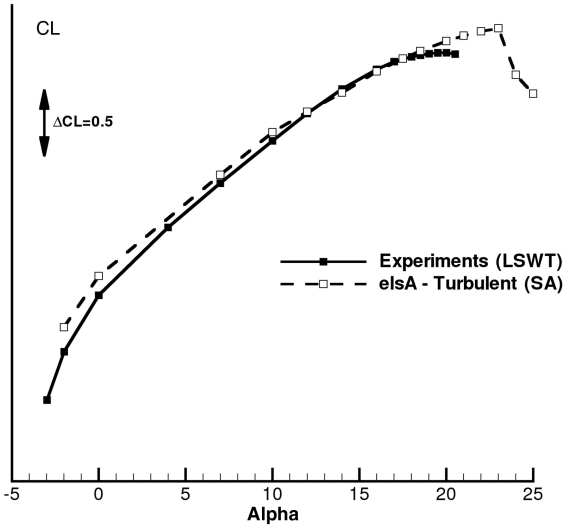

Fig. 5 Lift coefficient (SA denotes Spalart–Allmaras).

in elsA for bypass, TS and CF transition, and laminar separation bubble predictions. Those considered relevant here are, namely, the Arnal–Habiballah–Delcourt criterion for TS instabilities, the C1 criterion for crossflow instabilities, and the Gleyzes–Habiballah criterion for 2-D short bubble transition.

These criteria are functions of the incompressible shape factor H_i, of an averaged Pohlhausen parameter $\bar{\Lambda}_2$, of the crossflow displacement integral length δ_2, and of the external turbulence level T_u. Integral lengths are directly computed from the velocity field, but the shape factor is obtained indirectly as a function of the Pohlhausen parameter. Based on the RANS flowfield, the process consists of

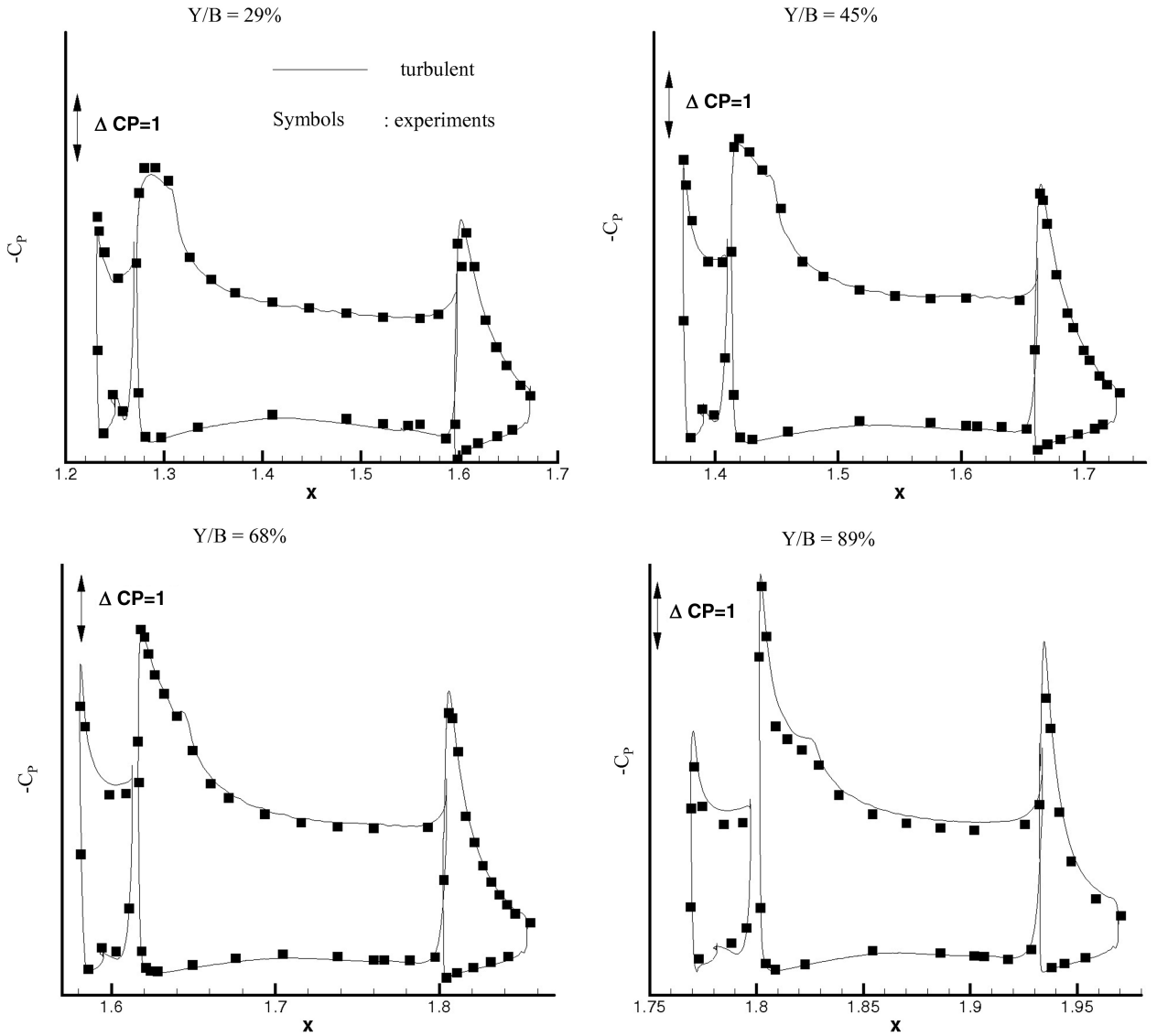

Fig. 6 Typical pressure distributions ($\alpha = 10$ deg.) on four sections.

estimating the boundary-layer parameters, then applying the criteria and using the concept of effective viscosity $\mu = \mu_L + \Gamma\mu_{\text{turb}}$, where Γ is the intermittency function ($\Gamma = 0$ for laminar and $\Gamma = 1$ for turbulent) and may be expressed as a (delayed) step function in its simplest form. Use of more sophisticated intermittency functions is being explored at ONERA.

The laminar part of the flow is imposed where the intermittency function is zero, then turbulence starts, usually some distance downstream of the detected transition location. The laminar flow region extends in the direction normal to the wall, up to about 1.3 times the boundary-layer thickness.

There was no prediction of attachment-line contamination in the version of elsA used for these computations, nor of relaminarization (these parts have been added since). An important hypothesis is that the boundary layer never extends outside the block in contact with the wall, in a normal to the wall direction. In a high-lift configuration, with regard to transition prediction, it is also assumed that there is no direct interaction between the two opposite boundary layers in the slot between elements.

A prerequisite in the introduction of transition prediction is the capacity to prescribe a transition location and hence to enforce a laminar part of the flow. This first condition was tested based on available information (i.e., transition measurements at one or two sections). In that case, transition was assumed at a constant X/C based on the instrumented sections.

Then computation was conducted with free transition over the slat outer surface, the wing lower side, and both sides of the flap. Over the wing upper side, it was necessary to impose a transition location because of numerical problems (which were due to a block boundary placed at a critical location and possibly an impact of small mesh distortions in the upper-wing leading-edge region). But experiments showed little evolution of transition on the wing upper side between 10 and 14 deg.

For this configuration and Reynolds number, there are no significant effects of taking transition into account during the computations on the pressure distributions, as shown in Figs. 7 and 8. On the upper surface, a slight increase of the local velocity is visible, especially on the outer section.

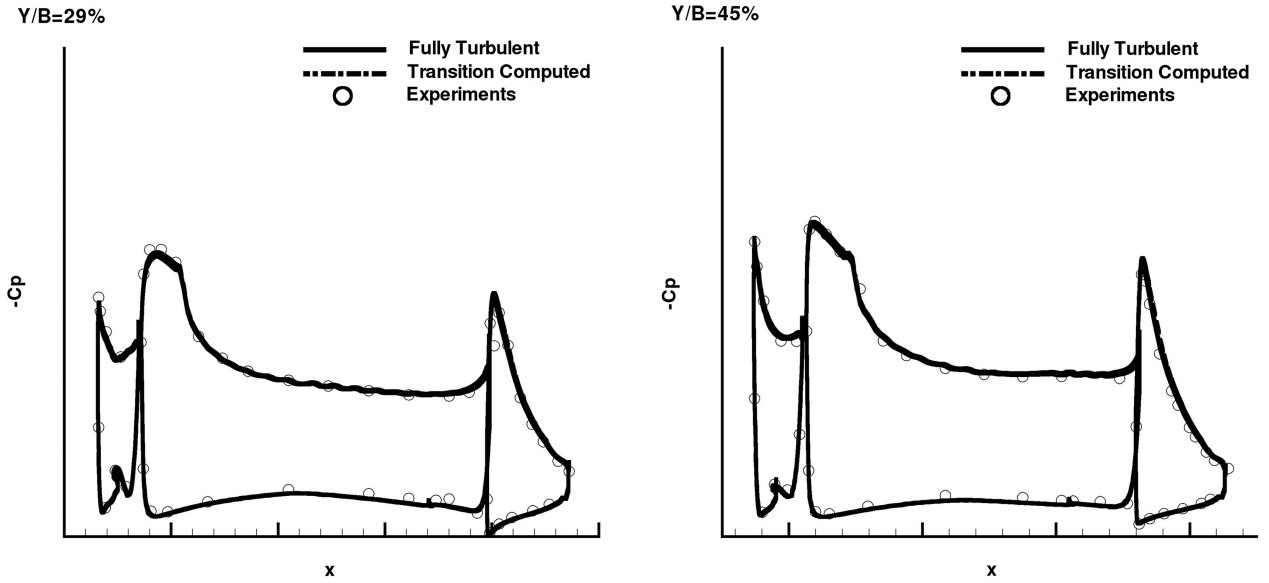

Fig. 7 Pressure distribution for sections 2 and 4; comparison with experiments ($\alpha = 10$ deg).

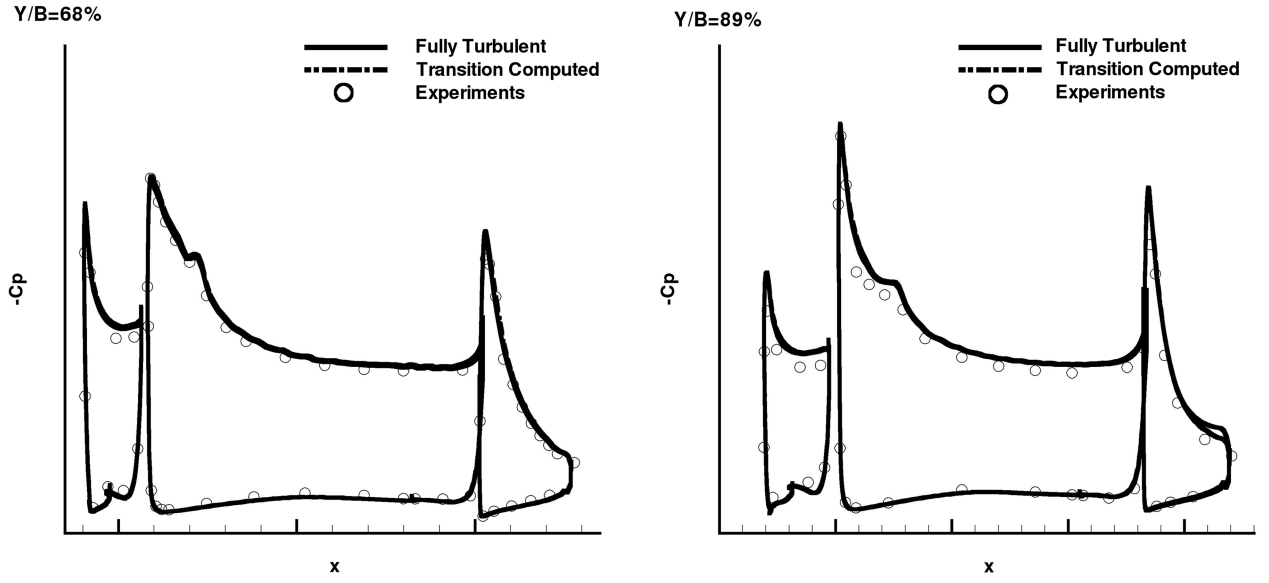

Fig. 8 Pressure distribution for sections 6 and 10; comparison with experiments ($\alpha = 10$ deg).

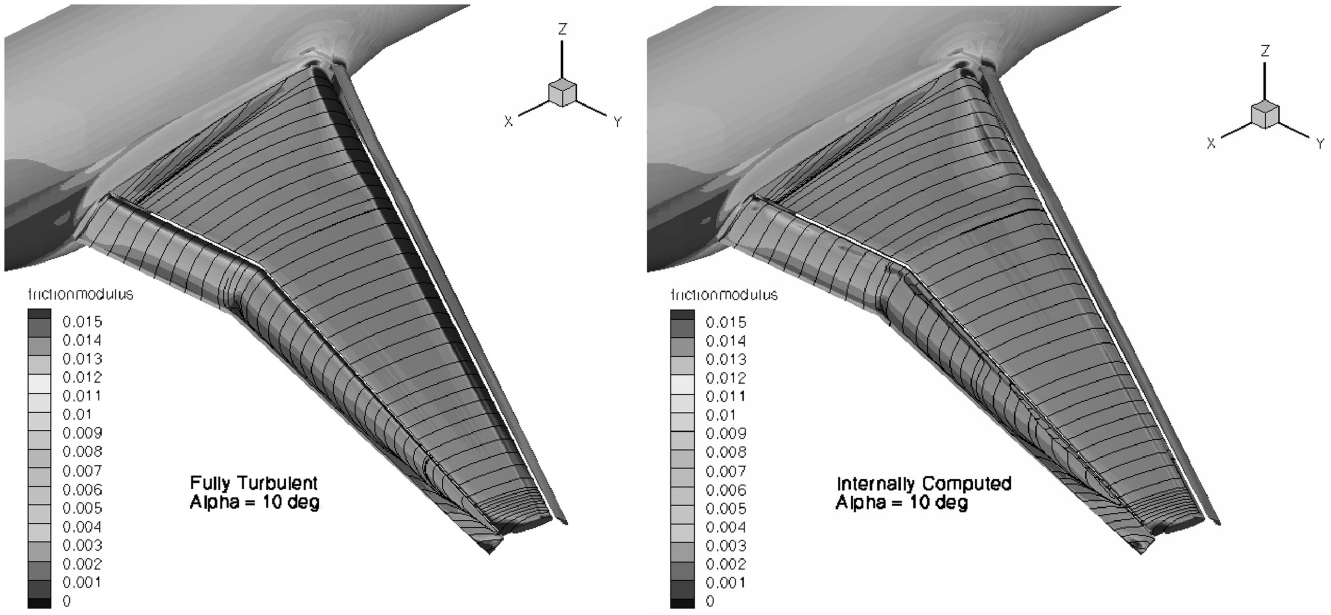

Fig. 9 Comparison fully turbulent; transition internally computed.

If there are no major differences observed on pressure distributions (Fig. 7 and 8), there are some when considering the friction. It can be seen in Fig. 9 that transition modifies not only the absolute value of skin-friction coefficient, particularly at the wing leading edge, but also the extent of the flow separation at the flap tip. In addition, it can be seen that a laminar separation bubble is computed on the flap upper surface in the outboard wing.

The relative variations of force coefficients from computations ($M = 0.174$ and $Re = 1.34 \times 10^6$) for an internally predicted turbulent transition at $\alpha = 10$ deg are $+1.45\%$ for ΔC_L and $+0.83\%$ for ΔC_D. However, at 10 deg, the global impact of transition on force coefficients is quite limited in that case, due to the preponderant contribution of pressure component to the total force for a high-lift configuration, as demonstrated in another task in EUROLIFT 2 (see [23]). The increase in lift coefficient observed with the introduction of transition is physically acceptable.

After successful computation at 10-deg incidence, extension toward the maximum-lift region was attempted. First tests were done with no modification of the upper-wing prescribed transition with the initial version of the transition-prediction tools in elsA, produced unsatisfying results because this transition location was too far downstream at large incidence, and the transition-prediction module could not deal with the block junction on the upper-wing region. The progress realized with the new version of elsA (presented in [6,7]) now allows transferring boundary-layer information and transition data across block boundaries. The KH3Y case was finally computed with this new version.

This computation, dedicated to the validation of the transition-prediction tools, was realized without contamination prediction (which later became available), because it is known from experimental data that contamination is followed with relaminarization and short bubble transition. In this case, the lower wing is computed with a transition region instead of being fully turbulent due to contamination, but the lower-wing flow has a small impact on global coefficients.

Results presented in Fig. 10 show the impact on $C_{L\max}$ and on stall of the various conditions. Vertical arrows on the figure indicate the location of $C_{L\max}$ in each case. Transition has almost no impact on the lift coefficient at 10 deg, confirming force-coefficient data. There is, in fact, almost no difference in lift coefficient in the linear range between transitional and turbulent results, whereas the impact of transition is quite important above 21 deg (stall being predicted at this incidence with transition). Stall, in this case, is caused by a progressive extension of midspan leading-edge separation, which does not connect to the wing trailing-edge separation. Taking into account transition visibly improves the prediction of stall and of $C_{L\max}$.

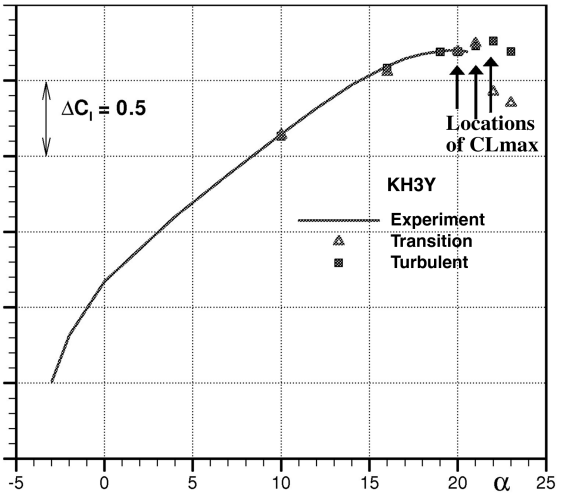

Fig. 10 $C_L(\alpha)$ with and without transition.

VI. Three-Dimensional RANS Boundary-Layer Coupling

As an intermediate step before automatic coupling to a boundary layer, the external weak coupling is necessary to explore and progressively extend the potential of this approach. Previous work in the EUROLIFT 1 project was based on the use of the surface pressure obtained in a fully turbulent RANS computation combined with the infinite swept-wing hypothesis, which was well adapted for the central part of the AFV wing [4].

In this preliminary work, the ONERA database method for TS and for traveling CF instabilities was extended and improved to be applicable to typical high-lift configurations. A further step explored now consists of suppressing the infinite swept-wing hypothesis and looking for a fully 3-D coupling. This involves the definition and detection of a boundary-layer outer limit, where the 3-D velocity components can be extracted to provide the input data for a 3-D boundary-layer computation.

Additionally, this process should allow the prediction of attachment-line contamination and of relaminarization. A necessary preliminary work consists of analyzing the mesh structure around the elements of interest and, from these, generating new data structures that are compatible with the viscous-layer extraction and boundary-layer inputs. In the present case, after eliminating the wing–fuselage junction, the wing comprises 48 sections in the spanwise direction, with 20 (respectively, 28) sections for the inner (respectively, outer) wing. Figures 11 and 12 show the mesh structure around the slat and the wing leading edges, with an approximate indication of the attachment-line location. In the case of the slat, the mesh remains more or less normal to the wall in this region. This is not verified in case of the wing: the mesh direction in this case is far from normal. In the spanwise direction, the sections represented here lay at about $\frac{3}{4}$ of the external wing (close to HF3 in Fig. 2).

For each element, these three blocks (visible in Figs. 11 and 12) were grouped into a single C mesh surrounding the element, allowing the determination of the outer limit of the viscous region. This was done using the coordinate system defined in Fig. 13, such that the x direction was normal to the leading edge. Then spanwise and total velocity gradients were used for defining the outer limit of the viscous region in the wall normal direction. The choice of coordinate system here was useful in allowing a more reliable estimation of the boundary-layer height and of directly providing the velocity components required for the estimation of both the contamination and the relaminarization parameters.

In the work presented, it was decided not to interpolate the field onto a new mesh, respecting rigorously normal to the leading edge and normal to the wall mesh directions. Hence, two hypotheses are necessary: that the mesh lines remain close enough to the wall normal direction to reduce geometrical distortions (the impact on the boundary-layer computation is a possible shift of the velocity

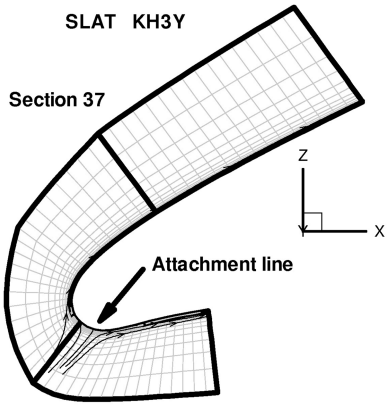

Fig. 11 Mesh structure around the slat.

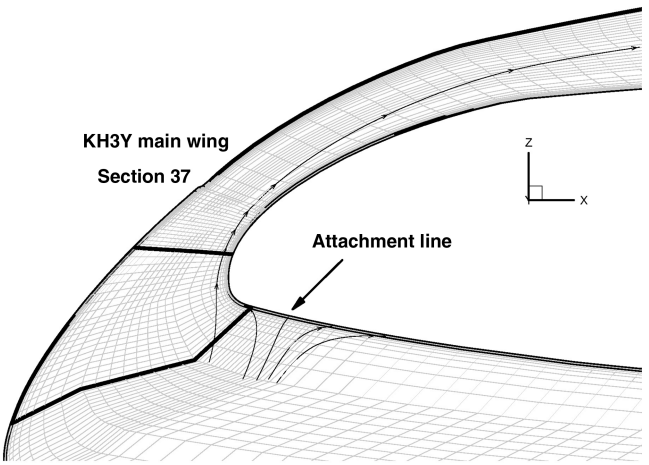

Fig. 12 Mesh structure around the wing.

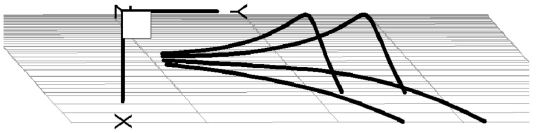

Fig. 13 Streamlines in the leading-edge region and selected coordinate system.

distribution, but boundary-layer equations are solved in their own local mesh, normal to the wall) and that around the attachment-line spanwise variations are slow enough to estimate normal to leading-edge components from the data on inclined-section mesh (Fig. 13). The first hypothesis is not respected for the main wing, but it was decided not to project the field onto a new mesh respecting these constraints. In the rotated coordinate system, the extracted velocity components directly give the spanwise and streamwise velocity components. As mentioned before, contamination prediction is based on

$$\bar{R} = W_e \Big/ \sqrt{\nu \frac{\partial U_e}{\partial X}}$$

and relaminarization is based on the parameter

$$K = \frac{\nu}{Q_e^2} \frac{\partial Q_e}{\partial s}$$

Estimation of these parameters was previously tested successfully on the rectangular AFV high-lift swept wing 4 and then applied to the KH3Y case.

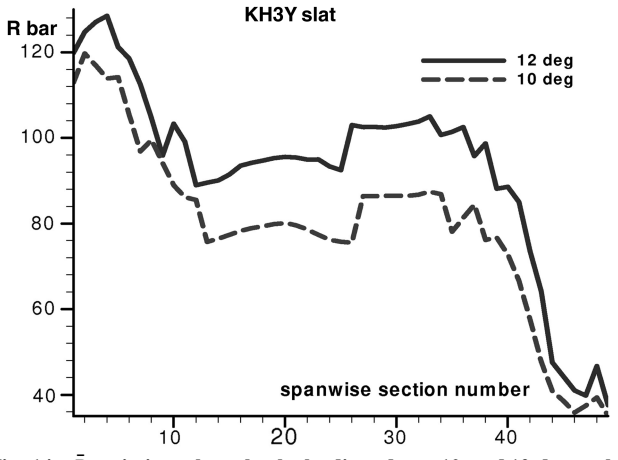

Fig. 14 $\bar{R}$ variations along the slat leading edge at 10- and 12-deg angles of attack.

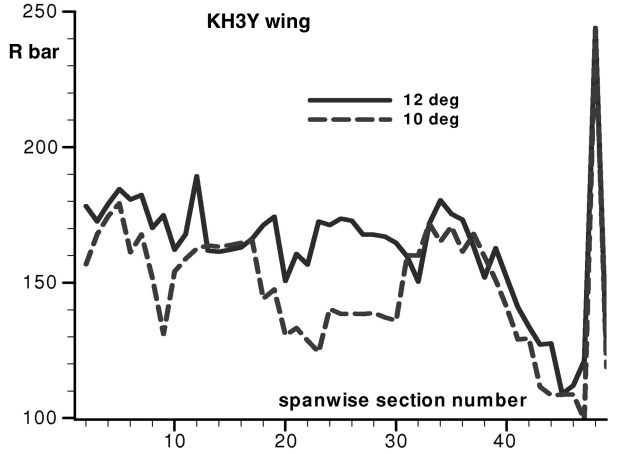

Fig. 15 $\bar{R}$ variations along the wing leading edge at 10- and 12-deg angles of attack.

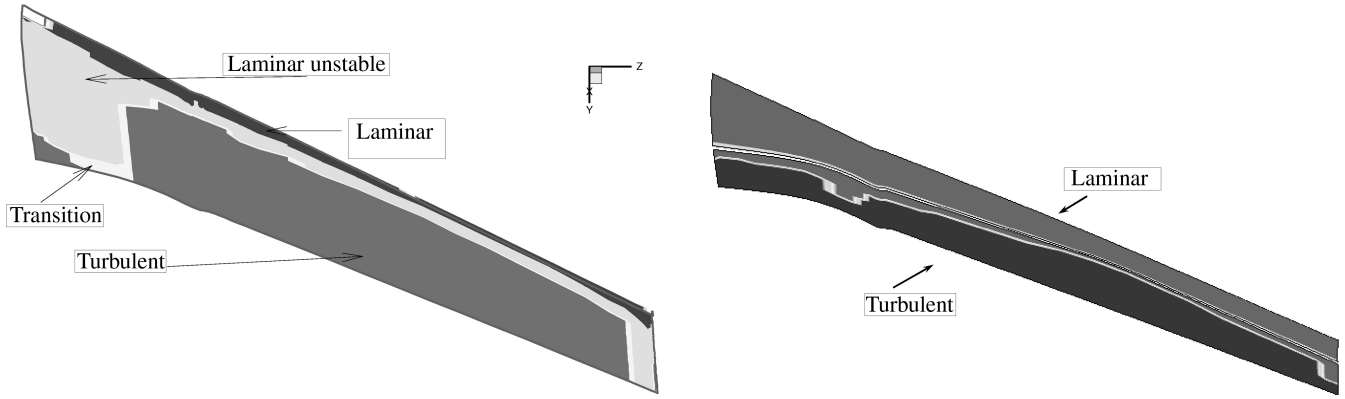

Fig. 16 Transition computed on the slat upper surface.

Figures 14 and 15 show the spanwise variations of the contamination Reynolds number. These results can be compared with the 2.5-D analysis that was performed for a single section and with the experimental results. On the slat, computed values are between 80 and 130, compared with 110 in the 2.5-D approach at 12-deg incidence. In the case of the wing, results are too small ($\bar{R} = 150$ instead of 200) in the 2.5-D approach at 10-deg incidence. Experimental results showed wing contamination at 12 deg of incidence and none at 10 deg. This underestimation is most probably a consequence of the mesh orientation at the wall (see Fig. 12). To check this, another partner in the project did a similar exercise but projected the field onto a wall normal mesh and was able to obtain results much closer to 200.

Velocity components at the boundary-layer edge were then used as input data for a 3-D boundary-layer calculation using the 3C3-D code [24] containing the ONERA database approach for transition prediction. Only the slat and main wing of the KH3Y wing were considered. The interface generated two surface meshes, upper and lower surfaces, corresponding to the selected surface elements (the slat lower surface goes from the attachment line to the slat kink and is neglected). The boundary-layer computation starts with a swept-wing similarity solution in the leading-edge region and then proceeds over the surface. Laminar boundary layer is computed up to either transition or laminar separation. The computation then proceeds to turbulent mode, provided that some compatibility conditions are respected.

Computation results are presented in Figs. 16 and 17. It can be seen that the transition location obtained with the boundary-layer approach and the database method lay in the same transitional area as those obtained from the internal transition detection tool in elsA, in case of the upper slat and the lower wing. One difference comes from the progressive transition in the boundary layer, as opposed to point transition in the RANS results.

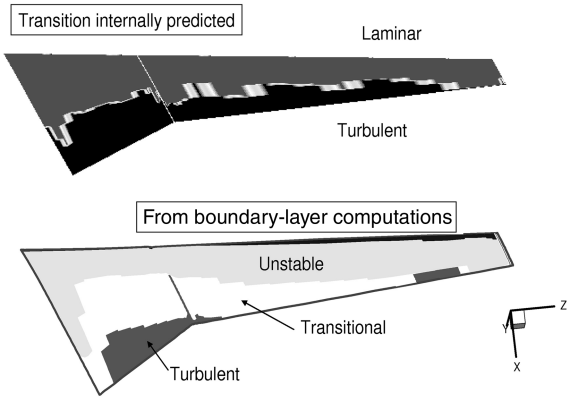

Fig. 17 Transition computed on the main wing lower surface at 10-deg incidence.

On the upper wing, the boundary-layer approach results in a very rapid separation resulting from a strong positive pressure gradient past the peak. In the RANS calculation, transition was prescribed at a fixed location because the block frontier is too close to where transition should occur. However, some differences remain when considering the nature of transition. For instance, on the slat upper surface, a transition due to the separation bubble is found from 3-D boundary-layer calculations, not with transition internally computed. This may result from the weaker coupling in the boundary-layer approach, but the 2-D separation criterion implemented in elsA may also be questionable for such applications. Also, the (relative) small number of mesh sections in the spanwise direction may cause some problems with this type of prediction. Weak coupling is acceptable in the C_L linear range, because pressure distribution is weakly affected by the transition location. This may not be true close to the maximum lift, in which case a better coupling procedure would be required.

VII. Conclusions

The characterization of the transition on a transport aircraft wing in a high-lift configuration was carried out using two approaches. The first method considers 3-D boundary-layer calculations based on a turbulent RANS mean flow solution through the use of a postprocessing tool, which can be used as an interface for a more general coupling procedure. This first approach allows the use of all available instability codes for transition prediction, local or nonlocal, linear or not, and is well adapted for detailed analysis of the transition phenomena.

The second method considers transition-prediction tools embedded in a RANS solver. The use of such a procedure makes it possible to consider a 3-D transition line on each surface of each element with no a priori knowledge of its location and is adapted to the corresponding flow solution during the convergence. This possibility is quite interesting from the user's point of view and is an important component for maximum-lift evaluation, where part of the wing can be separated, leading to a three-dimensional transition line in that case. Although the first implementation of this method showed important limitations when applied to these high-lift configurations, the new implementation proves to be much more general in scope and easier to put into use. The computational cost may remain quite important when starting from a converged turbulent solution, but the possibility of starting the computation with transition from the first iteration was also successfully tested. The specific transition-prediction tools in elsA are capable of predicting transition in a separation bubble, contrary to methods based on boundary-layer coupling. The evaluation of the shape factor requires a dense distribution of mesh points on the surface in the direction of the mean flow but does not require a large number of points in the boundary layer.

The next step to consider now is to evaluate in detail the impact of transition (internally computed) on maximum lift and to evaluate the Reynolds number effect on $C_{L\max}$ for a realistic high-lift configuration. The first evaluation of this Reynolds number effect

was considered on a clean-wing configuration within EUROLIFT 2 and will be considered for high-lift configurations after the end of the project.

Acknowledgments

The results presented in this paper have been obtained within the European research project EUROLIFT 2 under contract AST3-CT-2004-502896, which was cofinanced by the European Union within the Sixth Research Framework Program. Much thanks to the following persons: Geza Schrauf and Heinz Jakob of Airbus-Deutschland, who provided the pressure distributions and contributed to the analysis of the experimental results, Ralf Mertins and Gery Vidjaja, also of Airbus-Deutschland, who produced the KH3Y structured mesh for the landing configuration. Thanks also to Raffaele Donelli, Pierluigi Iannielli, and Ardeshir Hanifi for their important role in the project.

References

[1] Hansen, H., Thiede, P., Rudnik, R., Moens, F., and Quest, J., "Overview About the European High Lift Research Program EUROLIFT," AIAA Paper 2004-767, Jan. 2004.

[2] Seraudie, A., Perraud, J., and Moens, F., "Transition Measurement on a Swept Wing in High Lift Configuration," *Aerospace Science and Technology*, Vol. 7, No. 8, Dec. 2003, pp. 569–576. doi:10.1016/j.ast.2003.04.001; also International Council for the Aeronautical Sciences, Paper 2002-197, 2002.

[3] Neitzke, K. P., "Using Advanced Measurement Techniques in High Lift Validation Experiments," Confederation of European Aerospace Associations (CEAS) Aerospace Aerodynamics Research Conference, Royal Aeronautical Society Paper 31, June 2003.

[4] Perraud, J., Seraudie, A., and Moens, F., "Transition on a High Lift Swept Wing in the European Project EUROLIFT," *Journal of Aircraft*, Vol. 41, No. 5, Sept. 2004, pp. 1183–1190. doi:10.2514/1.4297

[5] Gazaix, M., Jollès, A., and Lazareff, M., "The elsA Object-Oriented Computational Tool for Industrial Applications," Proceedings of the 23rd Conference of the International Council for the Aeronautical Sciences, Toronto, Canada, International Council for the Aeronautical Sciences, Paper 2002-1.10.3., Sept. 2002.

[6] Cliquet, J., Houdeville, R., and Arnal, D., "Application of Laminar-Turbulent Transition Criteria in Navier-Stokes Computation," AIAA Paper 2007-515, Jan. 2007.

[7] Cliquet, J., and Houdeville, R., "Laminar-Turbulent Transition Criteria in the elsA Navier-Stokes Solver with Application to Complex Geometries," 2nd European Conference for Aerospace Sciences (EUCASS 2007), Brussels, Belgium, ONERA Paper TP 2007-130, July 2007.

[8] Cliquet, J., "Calcul de la Transition Laminaire-Turbulent dans les Codes Navier–Stokes. Application aux Géométries Complexes," Ph. D. Dissertation, Ecole Nationale de l'Air et de l'Espace, Toulouse, France, Oct. 2007.

[9] Toulorge, T., Ponsin, J., Perraud, J., and Moens, F., "Automatic Transition Prediction for RANS Computations Applied to a Generic High-Lift Wing," AIAA Paper 2007-1086, Jan. 2007.

[10] Krumbein, A. M., "Automatic Transition Prediction and Application to Three-Dimensional Wing Configurations," *Journal of Aircraft*, Vol. 44, No. 1, 2007, pp. 119–133. doi:10.2514/1.22254

[11] Krumbein, A. M., "Automatic Transition Prediction and Application to Three-Dimensional High-Lift Configurations," *Journal of Aircraft*, Vol. 44, No. 3, 2007, pp. 918–926. doi:10.2514/1.25528

[12] Moens, F., Perraud, J., Krumbein, A., Toulorge, T., Iannelli, P., Eliasson, P., and Hanifi, A., "Transition Prediction and Impact on a 3-D High-Lift Wing Configuration," *Journal of Aircraft* (to be published); also AIAA Paper 2007-4302, June 2007.

[13] Pfenninger, W., "Flow Phenomena at the Leading Edge of Swept Wings," *Recent Developments in Boundary Layer Research*, NATO AGARD-AG-97, Pt. 4, Paris, May 1965.

[14] Poll, D. I. A., "Some Aspects of the Flow Near a Swept Attachment Line with Particular Reference to Boundary Layer Transition," Cranfield Inst. of Technology, Rept. 7805, Cranfield, England, U.K., Aug. 1978.

[15] Beasley, J. A., "Calculation of the Laminar Boundary Layer and Prediction of Transition on a Sheared Wing," Royal Aeronautical Establishment, Rept. 3787, Farnborough, England, U.K., Oct. 1973.

[16] Arnal, D., and Juillen, J. C., "Leading Edge Contamination and Relaminarization on a Swept Wing at Incidence," *Numerical and Physical Aspects of Aerodynamic Flows IV*, edited by T. Cebeci, Springer–Verlag, Berlin, 1990, pp. 391–402.

[17] Arnal, D., "Three-Dimensional Boundary Layers: Laminar-Turbulent Transition," *Computations of Three-Dimensional Boundary Layers Including Separation*, AGARD, Rept. 741, Neuilly-sur-Seine, France, 1986, pp. 1–34.

[18] Arnal, D., "Transition Prediction in Transonic Flow," *IUTAM Symposium Transsonicum*, edited by J. Zierep and H. Oertel, Springer–Verlag, Berlin, 1988, pp. 253–262.

[19] Casalis, G., and Arnal, D., "ELFIN II Subtask 2.3: Data Base Method: Development and Validation of the Simplified Method for Pure Crossflow Instability at Low Speed," ONERA Rept. RF 119/5618.16, Dec. 1996.

[20] Gregory, N., Stuart, J. T., and Walker, W. S., On the Stability of Three Dimensional Boundary Layer with Application to the Flow Due to a Rotating Disc, *Philosophical Transactions of the Royal Society of London, Series A: Mathematical and Physical Sciences*, Vol. 248, No. 943, 1955, pp. 155–199. doi:10.1098/rsta.1955.0013

[21] Gaster, M., "A Note on the Relation Between Temporally Increasing and Spatially Increasing Disturbances in Hydrodynamic Stability," *Journal of Fluid Mechanics*, Vol. 14, 1962, pp. 222–224. doi:10.1017/S0022112062001184

[22] Gleyzes, C., Cousteix, J., and Bonnet, J. L., "Theoretical and Experimental Study of Low Reynolds Number Transitional Separation Bubbles," *Conference on Low Reynolds Number Airfoil Aerodynamics*, CP-77B123, edited by Th. J. Mueller, Univ. of Notre Dame, Dept. of Aerospace and Mechanical Engineering, Notre Dame, IN, June 1985.

[23] Esquieu, S., Méheut, M., von Geyr, H. F., and Brodersen, O., "Far-Field Drag Extraction from Numerical Solutions and Wake Surveys," 7th ONERA-DLR Aerospace Symposium, Toulouse, France, ONERA, TP 2006-155, Oct. 2006.

[24] Houdeville, R., Mazin, C., and Corjon, A., "Method of Characteristics for Computing Three-Dimensional Boundary Layers," *La Recherche Aerospatiale: Bulletin Bimestriel de l'Office National d'Etudes et de Recherches Aerospatiales*, Vol. 1, 1993, pp. 37–49.